Nonlinear Processes in Geophysics (1994) 1: 172 - 181

Nonlinear Processes in Geophysics

Distribution of incremental static stress caused by earthquakes

Y.Y. Kagan

Institute of Geophysics and Planetary Physics, University of California, Los Angeles, California 90024-1567, USA

Received 3 December 1993 - Accepted 21 March 1994 - Communicated by S. Lovejoy

Abstract. Theoretical calculations, simulations and measurements of rotation of earthquake focal mechanisms suggest that the stress in earthquake focal zones follows the Cauchy distribution which is one of the stable probability distributions (with the value of the exponent α equal to 1). We review the properties of the stable distributions and show that the Cauchy distribution is expected to approximate the stress caused by earthquakes occurring over geologically long intervals of a fault zone development. However, the stress caused by recent earthquakes recorded in instrumental catalogues, should follow symmetric stable distributions with the value of α significantly less than one. This is explained by a fractal distribution of earthquake hypocentres: the dimension of a hypocentre set, δ, is close to zero for short-term earthquake catalogues and asymptotically approaches $2\frac{1}{4}$ for long-time intervals. We use the Harvard catalogue of seismic moment tensor solutions to investigate the distribution of incremental static stress caused by earthquakes. The stress measured in the focal zone of each event is approximated by stable distributions. In agreement with theoretical considerations, the exponent value of the distribution approaches zero as the time span of an earthquake catalogue (ΔT) decreases. For large stress values α increases. We surmise that it is caused by the δ increase for small inter-earthquake distances due to location errors.

1 Introduction

The knowledge of tectonic stress in the lithosphere is an important ingredient for our understanding of earthquake mechanics and the interaction between earthquakes. Several techniques now exist for measuring stress in-situ (Hickman, 1991; Zoback, 1992). These methods however usually do not have the resolution and accuracy necessary to study the stress variation in the earthquake focal zone. Large rotations of the earthquake focal mechanisms indicate that the stress field responsible for earthquake generation in seismogenic zones is highly variable and heterogeneous (Kagan, 1992). In this work we study the incremental stress caused by earthquakes. Measurements of static displacements due to large earthquakes indicate that there is agreement between the experimental results and theoretical calculations which use the dislocation model in a half-space (cf. Bock et al., 1993). Reliable and extensive earthquake data which allow the incremental stress calculations extend for only 15-20 years. Thus we are observing only a short time interval in the development of earthquake fault zones the history of which is sometimes measured in millions of years. The above factors call for a statistical interpretation of the stress data: averaging over large tectonic areas we might infer the general properties of stress and its influence on earthquakes.

Statistical investigations of the world-wide pattern of static incremental stress present several problems: it is not clear at what points the stress should be evaluated for further study. A seemingly obvious solution – to compute the stress on a lattice of points distributed uniformly over the 3-D space – will not work since earthquake hypocentres or centroids (see a more detailed explanation of these terms in the next section) are concentrated on a fractal set (Kagan and Knopoff, 1980; Kagan, 1991). Thus the great majority of lattice points would be far away from any earthquake and hence have a zero incremental stress. We could select certain seismogenic zones for the study, but in this case the results would be strongly dependent on the selection criteria used. The only way to make the results independent of the arbitrary boundaries of the zones is to calculate the stress field at special points – at the positions of past earthquakes. This is similar to the approach proposed by Mandelbrot (1983) for a definition of point density for fractal sets: unconditional density cannot be defined, whereas the conditional density – measured around each point of the set – has a well-defined limit.

Geometric structures of earthquake focal zones exhibit great variability of an essentially stochastic character. In a series of papers (Kagan and Knopoff, 1980; Kagan, 1982; Kagan, 1991) we showed that earthquake hypocentres form a fractal set; for shallow earthquakes, the dimension increases with the time span of an earthquake catalogue (ΔT) approaching the limit of $2\frac{1}{4}$. Although a planar earthquake fault is a reasonable description of earthquake geometry in the first approximation, a detailed investigation shows the faults form a complex branching pattern governed by the Cauchy rotational distribution (Kagan, 1982). The Cauchy law has been proposed to describe the random stress caused by defects in the medium (Zolotarev and Strunin, 1971; Zolotarev, 1986; Kagan, 1990). The measurements of the correlations of earthquake focal mechanisms confirmed that the focal rotation also has the Cauchy distribution (Kagan, 1992). This leads to the conclusion that the presence of old earthquake fractures contributes to the randomness of the stress in an earthquake focal zone which in its turn generates new, more complex patterns of earthquake rupture.

However, the above papers had two drawbacks: a) the stress was not investigated directly, its properties were inferred through the geometry of earthquake hypocentres and focal mechanisms; b) we investigated long-term properties of earthquake geometrical patterns. In this work, we investigate the stress caused by earthquakes recorded in the catalogues of seismic moment tensor solutions, hence we are able to study not only the stress distribution but also to investigate its dependence on time.

2 Earthquakes and stress

As a first approximation, an earthquake may be represented by a sudden shear planar failure – appearance of a large dislocation loop (Aki and Richards, 1980) in rock material. In Fig. 1a we show a fault-plane trace on the surface of the Earth (similar to viewing from above an earthquake occurring on the San Andreas fault). Earthquake rupture starts at the hypocentre (the epicentre is a projection of the hypocentre on the Earth's surface), and propagates with velocity close to that of shear waves (3.0–4.5 km/s). As a rule, the hypocentre is situated at one end of the rupture area, thus its position is accidental with regard to the earthquake focal zone. The centroid is in the centre of the ruptured area, its position being determined by seismic moment tensor inversion (Dziewonski et al., 1993). As a result of the rupture two sides of the fault surface are displaced relative to each other in the direction of the arrows, for large earthquakes the displacement is of the order of a few meters.

Figure 1b shows a graphic representation of an earthquake source: quadrupolar radiation patterns characteristic of earthquakes. Standard seismological focal plots involve painting on a sphere, the sense of the first motion of P-waves, solid for compressional motion and open for dilatational. Two orthogonal planes separating these areas are the fault and auxiliary planes. In the routine determination of focal mechanisms it is impossible to distinguish between these planes.

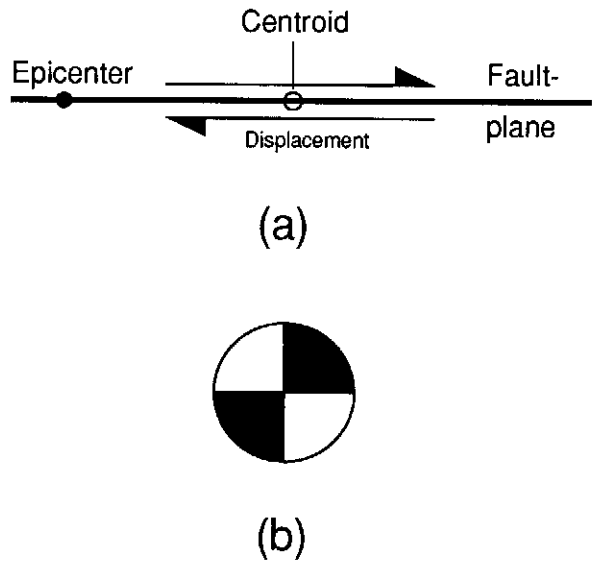

Fig. 1. Schematic diagrams of earthquake focal mechanism. (a) Fault-plane trace on the surface of the Earth. Earthquake rupture starts at the point on the fault-plane called the hypocentre (epicentre is the projection of a hypocentre on the Earth surface). (b) Equal-area projection (Aki and Richards, 1980, p. 110) of quadrupole radiation patterns.

The earthquake data are assembled in catalogues. The most complete and homogeneous at the present time is the worldwide catalogue of moment tensor inversions compiled by the Harvard group (Dziewonski et al., 1993). The available Harvard catalogue covers the period from January 1, 1977, to December 31, 1992, and contains more than 10,000 events. As an example of earthquake data, in Fig. 2 we display focal mechanisms for earthquakes in the Southern California area. (In this case we use preliminary Harvard data to display the recent January 17, 1994 Northridge, California earthquake.) Lower hemisphere diagrams of focal spheres are shown; the diagrams can be seen as 3-D rotations of the mechanism shown in Fig. 1b. The diagram shows that earthquakes are not concentrated only on a few well-known faults and the mechanisms of neighbouring events may have very different orientations, i.e., they undergo large 3-D rotations.

We use the earthquakes shown in Fig. 2 as well as earthquakes in surrounding areas to calculate the incremental static stress at the surface. For most stress calculations we use Okada's (1992) programme for a point

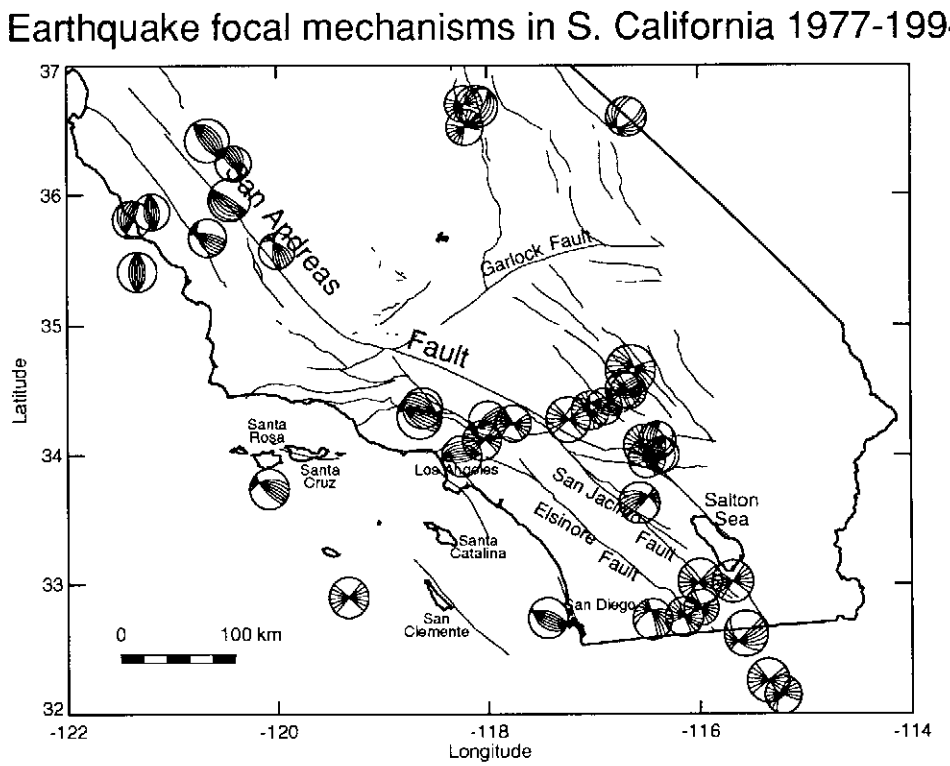

Fig. 2. Focal mechanisms of earthquakes from the 1977-1994 Harvard list in the Southern California area and major surface faults: latitude limits 32.0-37.0 N, longitude limits 114.0-122.0 W. Lower hemisphere diagrams of focal spheres are shown, the diagrams can be thought of as 3-D rotations of the mechanism shown in Fig. 1b. Size of a symbol is proportional to earthquake magnitude.

fault. However, for computation of stress caused by earthquakes with magnitude 6.5 and larger (including the Landers, 1992 earthquake, and the Superstition Hills earthquake of 1987) we use Okada's (1992) programme for a rectangular earthquake fault. We subdivide the known rupture surface into several patches and calculate the stress increments due to all fault patches.

In Fig. 3, we show the cumulative stress change of the first stress invariant (I_1) (average normal stress, see Eq. 14 below) for Southern California from 1977 to the present. Stress is evaluated at a surface. The distribution of the stress is dominated by the Landers 1992 earthquake (Stein et al., 1992). The incremental stress pattern in all the maps forms a complex mosaic due to the interaction of incremental stress fields of many earthquakes. The complex character of stress once again underscores the necessity of analysing the data statistically.

3 Stable probability distributions

Two properties of the stable probability distributions are of special interest for us: a) the sum of variables distributed according to any of the stable distributions has again the same type of probability distribution (the normal, or Gaussian distribution, which is one of the stable distributions, is the best known example of such behaviour); b) for most distributions, their tails decay according to a power law, hence the stable distributions underlie many fractal patterns (Mandelbrot, 1983). Except for a few cases, the stable distribution density does not have analytical form; however, their characteristic function can be expressed by a simple formula. The characteristic function is the Fourier (or Laplace) transform of a statistical distribution, and there is a one-to-one correspondence between both functions.

The general form of the characteristic function for a stable distribution is (Zolotarev, 1986)

$$\log \phi(\zeta, \alpha, \beta, \lambda, \gamma) = \lambda\left[i\zeta\gamma - |\zeta|^{\alpha} + i\zeta\omega(\zeta, \alpha, \beta)\right], \qquad (1)$$

with $0 < \alpha \leq 2$, $-1 \leq \beta \leq 1$, $-\infty < \gamma < \infty$, $\lambda > 0$, and

$$\omega(\zeta, \alpha, \beta) = \begin{cases} |\zeta|^{\alpha-1}\beta \tan\left(\frac{\pi}{2}\alpha\right), & \text{if } \alpha \neq 1, \\ -\beta\frac{2}{\pi}\log|\zeta|, & \text{if } \alpha = 1. \end{cases} \qquad (2)$$

In these formulae the exponent α is the main parameter of a stable distribution which characterises its form, γ is a shift parameter, λ is a scale parameter, β is the degree of the distribution asymmetry, $\beta = 0$ corresponds to a symmetric distribution. We use

$$\phi(\zeta, \alpha) = \phi(\zeta, \alpha, 0, 1, 0). \qquad (3)$$

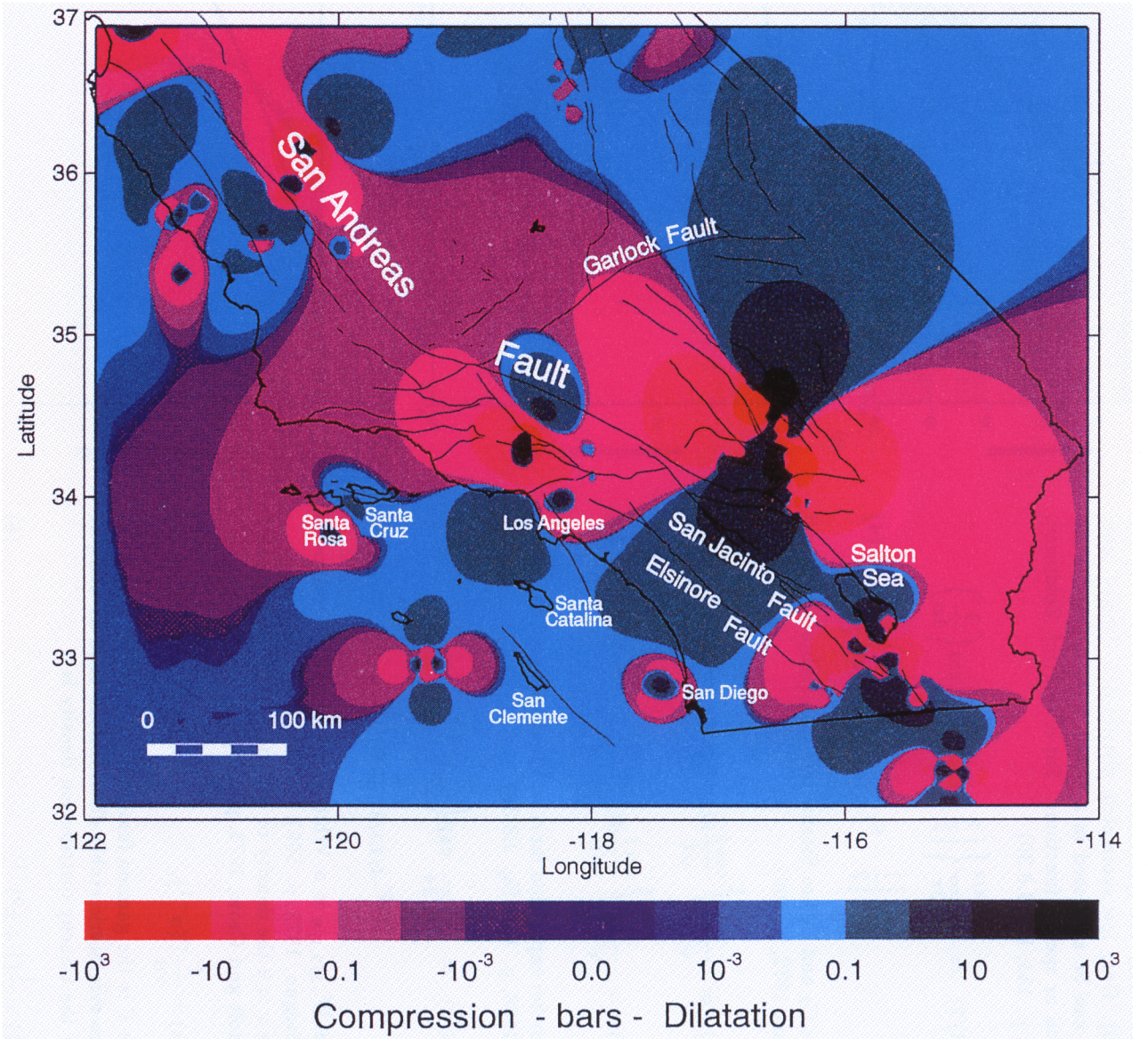

Fig. 3. Stress (invariant I_1) in S. California 1977-1994

It can be shown (see below) that the stress distribution follows a symmetric pattern. Thus below we consider only the symmetric distributions ($\beta = 0$, and $\gamma = 0$). Only few symmetric distribution density functions can be expressed in a closed form, using the analytical or special functions. For $\alpha = \frac{1}{2}$ (cf. Zolotarev, 1986, p. 155, Eq. 2.8.30)

$$f(x,1/2) = \frac{x^{-3/2}}{\sqrt{2\pi}}\left\{\left[\frac{1}{2} - C_2\left(\frac{1}{4x}\right)\right]\cos\left(\frac{1}{4x}\right) + \left[\frac{1}{2} - S_2\left(\frac{1}{4x}\right)\right]\sin\left(\frac{1}{4x}\right)\right\}, \quad (4)$$

where C_2 and S_2 are Fresnel integrals (Abramovitz and Stegun, 1972, p. 300).

$$C_2(x) = \frac{1}{\sqrt{2\pi}}\int_0^x \frac{\cos t}{\sqrt{t}}dt;$$

$$S_2(x) = \frac{1}{\sqrt{2\pi}}\int_0^x \frac{\sin t}{\sqrt{t}}dt. \quad (5)$$

Another expression for $\alpha = \frac{2}{3}$ is also quoted by Zolotarev (1986, p. 157, Eq. 2.8.32)

$$f(x,2/3) = \frac{x^{-1}}{2\sqrt{3\pi}}\exp\left(\frac{2}{27}x^{-2}\right) \times W_{-1/2,1/6}\left(\frac{4}{27}x^{-2}\right), \quad (6)$$

where $W_{-1/2,1/6}$ is a Whittaker function (Abramovitz and Stegun, 1972, p. 505).

For $x = 0$ the density in (4) and (6) can be evaluated by (Holt and Crow, 1973, p. 148)

$$f(0,\alpha) = \frac{1}{\pi\alpha}\Gamma(\alpha^{-1}), \quad (7)$$

where Γ is the gamma function.

Two symmetric stable distributions have an analytic form: the Cauchy distribution density is

$$f(x,1) = \frac{1}{\pi}(1+x^2)^{-1}, \quad (8)$$

and the Gaussian stable distribution density is

$$f(x,2) = \frac{1}{2\sqrt{\pi}}\exp\frac{-x^2}{4}. \quad (9)$$

The distributions (4) and (6) have been evaluated using the MATHEMATICA package (Wolfram, 1991). Holt and Crow (1973) calculated four-decimal tables of the stable distributions for $\alpha = 0.25(.25)2.00$ and $\beta = -1.00(.25)1.00$. In Fig. 4 we display distributions (4), (6), (8), and (9), as well as two symmetric distributions from Holt and Crow (1973) compilation: for $\alpha = 0.25$ and $\alpha = 0.75$. Cumulative curves for these distributions are obtained by numerical integration. Since

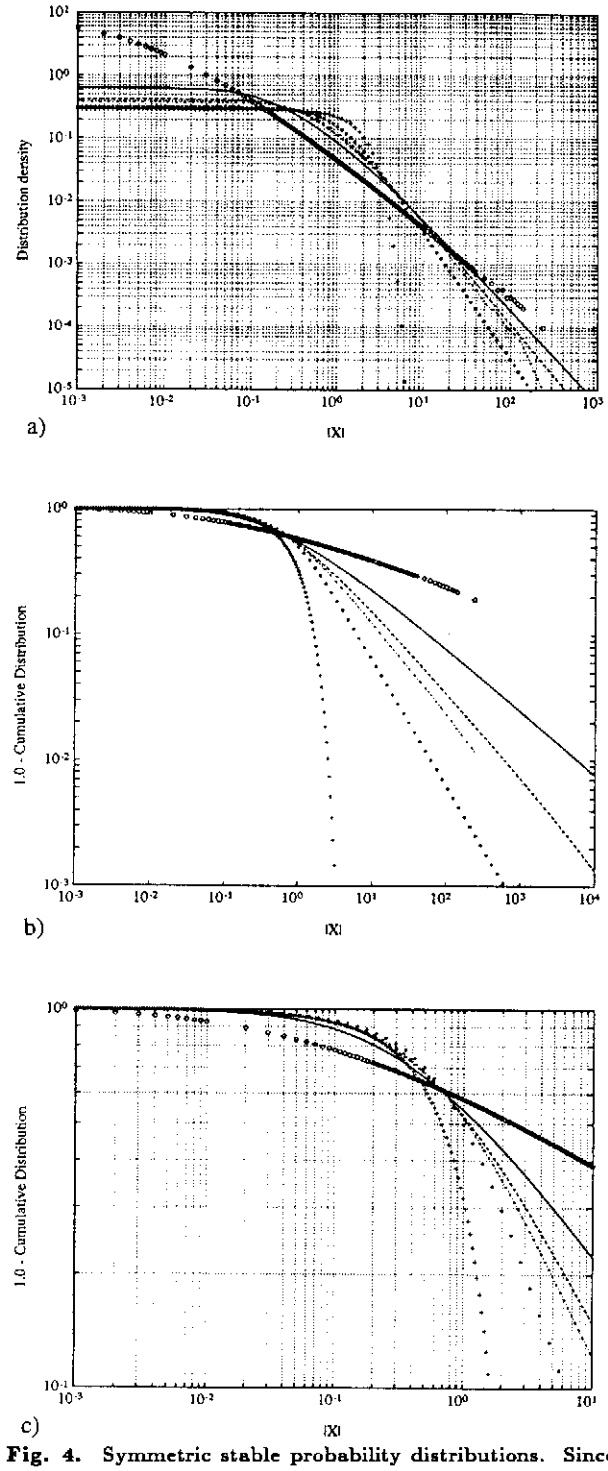

Fig. 4. Symmetric stable probability distributions. Since the distributions are symmetric, we consider absolute values of X. The value of exponent α is

- 1/4 – 'o' symbols;
- 1/2 – solid line;
- 2/3 – dashed line;
- 3/4 – dashdot line;
- 1 – '*' symbols (the Cauchy distribution);
- 2 – '+' symbols (the Gaussian distribution).

(a) Distribution density.
(b) Cumulative functions.
(c) Cumulative functions, enlargement of (b).

the distributions are symmetric, we calculate and display them for the absolute value of the argument. Except for the Gaussian law, which is a special case, distribution tails decay according to a power law:

$$f(x,\alpha) \propto x^{-\alpha-1}, \quad \text{for} \quad x \to \infty, \tag{10}$$

for the distribution density, and

$$1 - F(x,\alpha) \propto x^{-\alpha}, \quad \text{for} \quad x \to \infty, \tag{11}$$

for the cumulative function F. The decay (10) signifies that all of these distributions do not have the first statistical moment (mean) for $\alpha \leq 1$, therefore we need some other method to compare random variables. One convenient way to compare the distributions is to use the median, i.e., abscissa of intersection of curves in Fig. 4c with the ordinate value 0.5 (the median for absolute values of $|X|$ corresponds to quartiles of a symmetric X distribution). Whereas for the Cauchy distribution $\frac{1}{2}$ of a sample should be concentrated between -1 and 1, for the stable distribution with $\alpha = \frac{1}{4}$ the range is larger: from -2.2 to 2.2. This means in effect that a variable which follows the Cauchy distribution is concentrated closer to zero; the Cauchy variable has fewer observations with very large values than, for example, the distribution with $\alpha = \frac{1}{4}$.

4 Stress theoretical distributions

The Green function σ for an individual earthquake is symmetric, $\sigma(-\mathbf{r}) = -\sigma(\mathbf{r})$, where $\mathbf{r}$ is the radius vector. We assume also that the distribution of earthquake hypocentres around each reference event is also symmetric on average. Thus the resulting stress distribution will also be symmetric, hence γ and β in (1) are both zero.

Zolotarev and Strunin (1971) and Zolotarev (1986) show that for any point in an elastic medium which is surrounded by defects, the characteristic function for the random stress distribution can be written as

$$\log \phi(\zeta,\alpha) = \int_0^\infty [\exp(i\zeta\sigma r^{-3}) - 1]\nu(r) r^2 dr, \tag{12}$$

where $\nu(r)$ is the density of defects which might depend on r, distance from the reference point, and σ is the normalized (for $r = 1$) stress Green function of an earthquake, stress decays with distance as r^{-3}.

Zolotarev's formula (12) has been derived for uniformly distributed defects of one and the same size (but possibly of different type), while seismic moments of earthquakes vary enormously (Kagan, 1993). Thus, averaging over seismic moments is necessary in (12). If one uses for seismic moment distribution, a power law (Pareto distribution), then its first and second moments are infinite and Zolotarev's (1986) conditions (see his Eqs. 1.1.10 and 1.1.11) are not satisfied. In reality the seismic moment distribution is a gamma law (Kagan, 1993), which has finite statistical moments, but the influence of strong earthquakes as shown in Fig. 3, is clearly predominant. However, for the global seismicity distribution we average over an ensemble of seismic zones, hopefully guaranteeing the stability of statistical estimates.

To simplify the notation, we display the distribution for only one component of a stress tensor; the distribution for any other component differs only by a scale factor. For the uniform 3-D distribution of defects $\nu = \nu_0$. However for the fractal distribution of sources $\nu = \nu_0 r^{\delta - D}$, where $D = 3$ is the Euclidean dimension of the space, and δ is a fractal correlation dimension of earthquake hypocentres (Kagan and Knopoff, 1980; Kagan 1991). Then (cf. Zolotarev 1986, Eq. 1.1.16)

$$\begin{aligned} \log \phi(\zeta,\alpha) &= \nu_0 \int_0^\infty [\exp(i\zeta\sigma u) - 1] u^{(\delta/3)-1} du \\ &= \nu_0 \Gamma(-\alpha) |\zeta|^\alpha, \end{aligned} \tag{13}$$

with $\alpha = \delta/3$. This means that if $\delta = 3$ the resulting distribution is the Cauchy law (8) (Zolotarev and Strunin, 1971; Zolotarev, 1986; Kagan, 1990), whereas for a fractal spatial distribution of earthquakes $\alpha < 1$.

5 Incremental stress measurements

Using Okada's (1992) programme for a point and extended dislocation in a half-space, we compute the combined incremental static stress in the focal zone of each shallow event (the depth range 0-70 km) with the magnitude greater than 5. There are 7903 such earthquakes in the worldwide Harvard list of 1977-1992, their centroids taken as reference points. However, in the stress calculation, we use earthquakes at all depths (since large events which are deeper than 70 km can still contribute a significant stress increment to shallower depths). The total number of all earthquakes is 10,566.

In Fig. 5 we display the histogram and the cumulative distribution for the first stress invariant (Jaeger and Cook, 1979, p. 23; Kagan, 1994)

$$I_1 = tr(s_{ij}) = s_{11} + s_{22} + s_{33}, \tag{14}$$

where s_{ij} is a stress tensor. For comparison, we also show three symmetric stable distributions, $\alpha = 1/2$, $2/3$, and 1. The theoretical curves are calculated using the scale factor $\lambda = 10^{-1.5}$, this value seems to approximate the experimental data reasonably well; we did not try to fit the histogram and the cumulative curve more closely to the theoretical curves for the reasons explained below. It is obvious from the plots, for example, that the I_1 distribution is more sharply peaked than the Cauchy law predicts. The difference between the theoretical and experimental curves is difficult to see in these diagrams, thus we produce another plot in which we use the symmetry of the stress distribution.

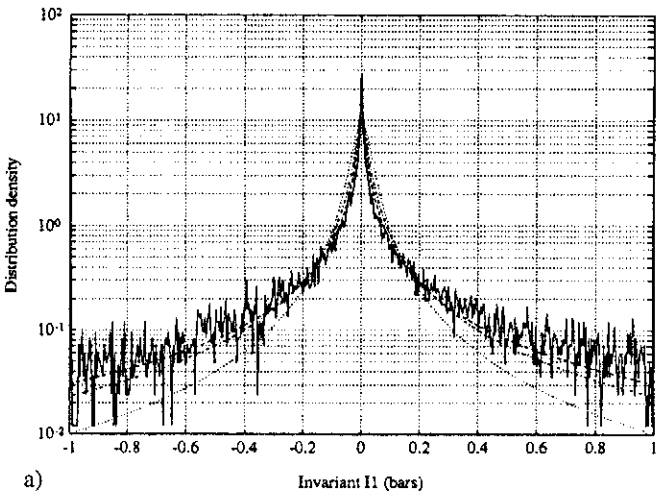

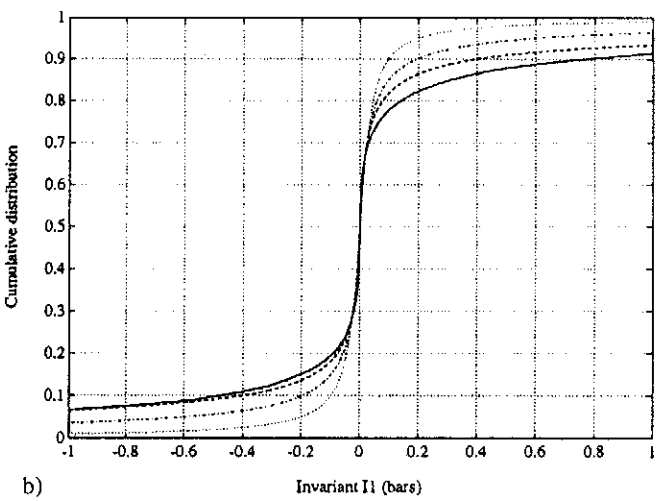

Fig. 5. Distribution of incremental stress invariant I_1 for worldwide shallow earthquakes in the Harvard catalogue. We calculate the incremental stress caused by earthquakes at all depths at a centroid point of any event in the depth range 0-70 km (see Figs. 2 and 3). The invariant corresponds to the sum of principal stresses, or to the mean normal stress. Positive values correspond to dilatation. The theoretical curves are calculated using the scale factor $\lambda = 10^{-1.5}$, the value of exponent α for these distributions are:

$$\begin{cases} 1/2 & \text{– dashed line;} \\ 2/3 & \text{– dashdot line;} \\ 1 & \text{– dotted line (the Cauchy distribution).} \end{cases}$$

(a) Theoretical distribution density and histogram for stress invariant I_1.
(b) Cumulative distributions.

According to the Coulomb failure criterion (Scholz, 1990; Kagan, 1994), we would expect the distribution of the average normal stress (I_1) to be highly asymmetric with more earthquakes occurring when the incremental stress is dilatational. Contrary to such expectations, the plots (Fig. 5) are almost symmetric. The cumulative curves (Fig. 5b) exhibit a slight preference for dilatational stress (for example, about 9% of earthquakes occur when $I_1 \geq 1.0$ bar whereas only about 7% of earthquakes occur with $I_1 \leq -1.0$ bar). However, the analysis of curves for various seismic regions (Kagan, 1994) shows that this asymmetry is not spatially or temporally consistent and could be explained by the stress random fluctuations.

Even if the distribution of the I_1 has a slight asymmetry, the distributions of stress tensor components should be symmetric, hence we might study their absolute values. In Fig. 6, we show several curves calculated for stress components $S = (|s_{11}| + |s_{12}| + |s_{22}|)/3$; these components have been selected since the horizontal components are larger than the vertical ones for shallow earthquakes (Kagan, 1994). We use the sum of three components to suppress random fluctuations. As we have explained earlier, the sum of stable variables is distributed according to the same stable distribution, as a single variable. For $\alpha < 1$ this would imply that the statistical moments of the sum would have a higher scatter than the moments of its components (the mathematical expectation for all the moments is infinity); however, in our case we are interested in the cumulative function fluctuations, and these fluctuations decay when we add several tensor components.

We calculate the incremental stress at the centroid point of each of the reference points for several subcatalogues: one curve is for a full Harvard list, i.e., for 10,566 earthquakes registered over 16 years, other curves are for the stress caused by earthquakes which are separated from a reference event by no more than 1250, 250, and 50 catalogue entries. This means that on the average we compute the stress caused by earthquakes in time intervals (ΔT) not exceeding 16, 1.9, 0.4, and 0.08 years.

Several possible sources of error need to be considered with regard to the experimental data. First, earthquake locations are greatly perturbed by location errors which randomise the position of earthquake centroids. This error is especially serious when distances between earthquakes are small. The location errors for modern worldwide earthquake catalogues are of the order of 10 km (Dziewonski et al., 1993). Second, the point model for an earthquake source is inappropriate for small distances. During a large earthquake, the rupture propagates over a plane-like volume of significant extent. Even if we use the Green function for an extended fault (Okada, 1992), the computed resulting stress pattern is a gross over-simplification. Shallow earthquakes are accompanied by a large number of aftershocks which are

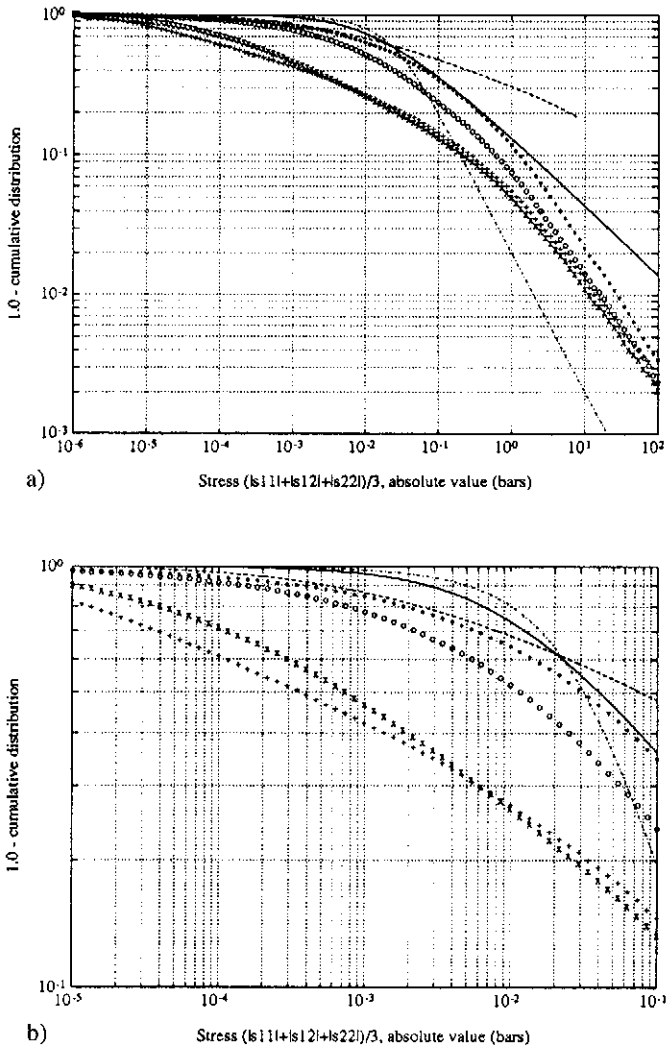

Fig. 6. Dependence of the distribution of stress component sum, $S = (|s_{11}| + |s_{12}| + |s_{22}|)/3$, on time interval between events. (b) plot is an enlargement of (a). The theoretical curves are calculated using the scale factor $\lambda = 10^{-1.5}$, the value of exponent α for these distributions are:

$$\begin{cases} 1/4 & \text{– dashed line;} \\ 1/2 & \text{– solid line;} \\ 1 & \text{– dashdot line (the Cauchy distribution).} \end{cases}$$

Stress increments are calculated:
for the full catalogue – stars;
for 1250 earthquakes before and after the reference event – circles;
for 250 earthquakes before and after the reference event – 'x'-es; and
for 50 earthquakes before and after the reference event – pluses.

concentrated in a focal zone, manifesting the large stress concentrations inside the zone. The measurements of surface displacement in the recent Landers earthquake (Sieh et al., 1993) demonstrate that the earthquake slip changes drastically over small fault distances. Hence there are very large residual stresses which remain after an earthquake.

When comparing the theoretical and experimental curves, we can vary the values of two adjustable parameters, that of α (index of a distribution) and of λ (scale factor). As we explained above, since the stress distribution is symmetric: $\beta = 0$ and $\gamma = 0$ (see Zolotarev's, 1986, formula 2.1.2), we can consider only absolute values of the variable. The change of λ causes a horizontal shift of theoretical curves in the diagrams in Fig. 6, whereas a modification of α leads to a change of the asymptotic slope of the curves for $x \to \infty$ (distribution tail), as well as to a change of the curvature in the left-hand part of the diagram (see also Figs. 4b,c). Since the λ parameter has not been evaluated and adjusted in Fig. 6, the curves can be arbitrarily shifted in a horizontal direction. For all the experimental curves, the distribution of stress for large abscissa values has a slope approaching one, hence they are closer to the Cauchy distribution. These large stresses are caused by near earthquakes, and the hypocentres of these earthquakes have a fractal dimension close to three due to location errors (Kagan and Knopoff, 1980; Kagan, 1991): That makes the behaviour of the curves at the right-hand tail of the distribution to be strongly influenced by location errors.

The experimental curves for small stress values are less influenced by the location errors discussed above. However, even for these curves it is not clear how to approximate them by theoretical stable distributions: we do not have a sufficient number of theoretical curves to fit the curves and infer the parameter values. As a preliminary solution, we measure a slope of linear parts of the experimental curves: according to (11), the slope in the loglog plot should correspond to α. In practical terms, we have used the following intervals to determine the slope (α) by visually fitting a straight line to the curves:

$\Delta T = 16$ yr,	1 – 100 bars,	$\alpha = 0.74$;
$\Delta T = 1.9$ yr,	10^{-2} – 3×10^{-1} bars,	$\alpha = 0.39$;
$\Delta T = 0.4$ yr,	10^{-3} – 10^{-1} bars,	$\alpha = 0.29$;
$\Delta T = 0.08$ yr,	10^{-4} – 10^{-2} bars,	$\alpha = 0.17$.

The earthquake fractal (correlation) dimension is dependent on the time span (ΔT) of a catalogue, for example, for a one day interval between earthquakes the dimension is $\delta \approx 1.0$, for 0.1 year interval $\delta \approx 1.5$, and for one year interval $\delta \approx 1.9$ (Kagan, 1991, Tables 2 and 3). According to (13) $\alpha = \delta/3$. Thus the α values versus ΔT should be as follows:

$\alpha = 0.75$ for $\Delta T = 23.5$ yrs;
$\alpha = 0.63$ for $\Delta T = 1$ yr;
$\alpha = 0.5$ for $\Delta T = 0.1$ yr;
$\alpha = 0.33$ for $\Delta T = 1/365$ yr.

Thus the predicted values of α exponent are similar to those obtained by fitting the curves to experimental distributions in Fig. 6: the largest discrepancies are for composite catalogues with small time intervals.

To test whether the replacement of an extended earthquake focal zone by a point source causes significant changes in the distributions, we performed similar stress calculations using the rectangular fault model by Okada (1992). There are several complications in this analysis. For the majority of earthquakes in the Harvard catalogue we cannot distinguish between the fault plane and the auxiliary nodal plane, thus the planes might be interchanged in about half of the cases. Moreover, the plane orientation is estimated with an error, over large distances this error might lead to a significant deviation of the calculated stress from its real values. The histograms we obtained by using the extended source approximation are found to be similar to those shown in Fig. 6.

6 Discussion

There are several consequences for the incremental stress to be distributed according to stable distributions with the index $\alpha \leq 1$. As we mentioned in section 3, since these distributions do not have finite statistical moments of any order, the average stress is infinite, i.e., cannot be meaningfully defined. To characterise the stress distribution we should use a median or other measure of a distribution scatter, i.e., quartiles, etc. The α value is lower for smaller inter-earthquake time intervals. This signifies that the random stress is more likely to be larger in the earthquake focal zone around the time of earthquake occurrence, than before or after the event. This stress increase might seem to be obvious, since most shallow earthquakes are accompanied by foreshocks and aftershocks, or are themselves foreshocks or aftershocks of some other event. Therefore, it is to be expected that this temporal and spacial earthquake clustering would result in strong stress concentrations. However, the above analysis quantifies these assumed inter-relations.

In deriving the theoretical distributions for the stress increments (13) we made several simplifying assumptions (Zolotarev and Strunin, 1971; Zolotarev, 1986; Kagan, 1990): for instance, earthquakes were taken to be independently distributed through the volume of rock. The presence of extensive aftershock sequences, among other evidence, points out that earthquakes are strongly interdependent, and it is generally assumed that the physical basis for this interdependence is stress increments caused by earthquakes. However, the results of statistical analysis of earthquake catalogues seems to confirm the prediction by (13) that the stress is distributed according to the stable distributions with the exponent $\alpha \leq 1$.

As we mentioned in section 3, the stable distributions have a certain property of 'self-replication': the sum of random stable variables is itself a stable variable. Consequently, we can assume that the distribution of sources in an earthquake focal zone is controlled by a stable distribution of stress in such a way that new sources (due to earthquake rupture, fault propagation and branching) again cause the new stress increments which are distributed according to the same stable distribution. We might interpret this fractal earthquake fault pattern created in the presence of large tectonic and lithostatic stresses, as a critical self-organization of earthquake faults (Bak and Chen, 1991, and references therein).

In our previous work (Kagan, 1982; Kagan, 1990), it was shown that a non-planarity of earthquake faults can be explained by the stress distribution due to earthquake sources and interaction of the incremental stress with the regional tectonic stress. The deviations of earthquake focal mechanisms from coherence are shown to be approximated by the Cauchy distribution (Kagan, 1992). On the other hand, this statistical distribution is the consequence of the simplest assumptions about the earthquake fault zone structure (see Eq. 13). Therefore, the stress interaction presents a plausible model for an earthquake generating process. The Cauchy distribution has $\alpha = 1$, thus our results in this work which suggest that $\alpha \leq 0.75$, seems to contradict the previous results. Several issues need to be taken into account in the comparison: 1) the difference between stable distributions with $\alpha = 1$ and $\alpha = 0.75$ is not large as exemplified by the diagrams by Holt and Crow (1973) and by Zolotarev (1986, his Fig. 3); 2) there is no equivalent for the *rotational* stable distribution with exponent 0.75, it is possible, that if such distribution were available, it would fit the experimental curves for rotation of earthquake focal mechanisms (Kagan, 1992) even better than the Cauchy rotational distribution; 3) rotation of earthquake focal mechanisms is the result of a very long process (millions of years) of tectonic deformation; it is possible that the correlation fractal dimension δ is larger than 2.25 for such intervals.

The above considerations do not take into account the dynamic processes during the earthquake rupture process. The dynamic stress increments impacting on the rock medium near the rupture front might be considerably higher (cf. Heaton, 1990) than the static stress changes we considered in this work. Thus the higher stress at the earthquake focal zone for a small time span of an earthquake catalogue, which is predicted by (13) and confirmed by our calculations (Fig. 6), might interact in the limit $\Delta T \rightarrow 0$ with the dynamic overstress due to the earthquake rupture. Their interaction then defines possible deflection of the rupture surface from pla-

nar propagation, i.e., branching of an earthquake fault, non-planar fault extension, and, in general, the formation of a complex earthquake fault zone.

Acknowledgements. This research was supported by Grant 93-40 IGPP-LLNL of the Lawrence Livermore National Laboratory. I acknowledge useful discussions held with D. D. Jackson of UCLA, J. B. Rundle of LLNL, and Y. Ben-Zion of Harvard University. I am especially grateful to reviewer V. F. Pisarenko (Moscow, Russia) for his useful remarks which significantly improved the manuscript. I wish to thank Dr. Y. Okada of the National Research Inst., Tsukuba, Japan for use of his half-space computer programmes. Publication 4127, Institute of Geophysics and Planetary Physics, University of California, Los Angeles.

References

Abramovitz, M., and Stegun, I. A., *Handbook of Mathematical Functions*, Dover, NY, pp. 1046, 1972.

Aki, K., and Richards, P., *Quantitative Seismology*, W. H. Freeman, San Francisco, 2 Vols, 557 and 373 pp., 1980.

Bak, P., and Chen, K., Self-organized criticality, *Scient. American, 264(1)*, 46–53, 1991.

Bock, Y., Agnew, D. C., Fang, P., Genrich, J. F., and others, Detection of crustal deformation from the Landers earthquake sequence using continuous geodetic measurements, *Nature, 361*, 337–340, 1993.

Dziewonski, A. M., Ekstrom, G., and Salganik, M. P., Centroid-moment tensor solutions for January-March, 1992, *Phys. Earth Planet. Inter., 77*, 143–150, 1993.

Heaton, T. H., Evidence for and implications of self-healing pulses of slip in earthquake rupture, *Phys. Earth Planet. Inter., 64*, 1–20, 1990.

Hickman, S. H., Stress in the lithosphere and the strength of active faults, *Rev. Geophys., 29*, 759–775, 1991.

Holt, D. R., and Crow, E. L., Tables and graphs of the stable probability density functions, *J. Res. Nat. Bureau Standards, B77*, 143–198. 1973.

Jaeger, J. C., and Cook, N. G. W., *Fundamentals of Rock Mechanics*, 3-rd ed., Chapman and Hall, London, 593 pp., 1979.

Kagan, Y. Y., Stochastic model of earthquake fault geometry, *Geophys. J. R. astr. Soc., 71*, 659–691, 1982.

Kagan, Y. Y., Random stress and earthquake statistics: spatial dependence, *Geophys. J. Int., 102*, 573–583, 1990.

Kagan, Y. Y., Fractal dimension of brittle fracture, *J. Nonlinear Sci., 1*, 1–16, 1991.

Kagan, Y. Y., Correlations of earthquake focal mechanisms, *Geophys. J. Int., 110*, 305–320, 1992.

Kagan, Y. Y., Statistics of characteristic earthquakes, *Bull. Seismol. Soc. Amer., 83*, 7–24, 1993.

Kagan, Y. Y., Incremental stress and earthquakes, *Geophys. J. Int.*, in press, 1994.

Kagan, Y. Y., and Knopoff, L., Spatial distribution of earthquakes: the two-point correlation function, *Geophys. J. Roy. astr. Soc., 62*, 303–320, 1980.

Mandelbrot, B. B., *The Fractal Geometry of Nature*, W. H. Freeman, San Francisco, Calif., 2nd edition, pp. 468, 1983.

Okada, Y., Internal deformation due to shear and tensile faults in a half-space, *Bull. Seismol. Soc. Amer., 82*, 1018–1040, 1992.

Scholz, C. H., *The Mechanics of Earthquakes and Faulting*, Cambr. Univ. Press, Cambridge, pp. 439, 1990.

Sieh, K., Jones, L., Hauksson, E., Hudnut, K., and others, Near-field investigations of the Landers earthquake sequence, April to July 1992, *Science, 260*, 171–176, 1993.

Stein, R. S., King, G. C. P., and Lin, J., Changes in failure stress on the Southern San Andreas fault system caused by the 1992 magnitude = 7.4 Landers earthquake, *Science, 258*, 1328–1332, 1992.

Wolfram, S., *Mathematica: a System for doing Mathematics by Computer*, 2nd ed., Addison-Wesley Pub. Co., pp. 961, 1991.

Zoback, M. L., 1st-order and 2nd-order patterns of stress in the lithosphere – the world stress map project. *J. Geophys. Res., 97*, 11703–11728, 1992.

Zolotarev, V. M., and Strunin, B. M., Internal-stress distribution for a random distribution of point defects, *Soviet Phys. Solid State, 13*, 481–482 (English translation), 1971.

Zolotarev, V. M., *One-Dimensional Stable Distributions*, Amer. Math. Soc., Providence, R.I., pp. 284, 1986.